

Polyimide for silicon solar cells with double-sided textured pyramids

Ngwe Zin^{a,b,*}, Keith McIntosh^c, Sara Bakhshi^a, Abraham Vázquez-Guardado^a, Teng Kho^b, Kean Fong^b, Matthew Stocks^b, Evan Franklin^b, Andrew Blakers^b

^a University of Central Florida, Orlando, FL 32768, USA

^b Australian National University, Canberra, ACT 2601, Australia

^c PV Lighthouse, Coledale, NSW 2515, Australia

ARTICLE INFO

Keywords:

Rear texture
Diffusions
Passivation
PECVD nitride
ALD AlO_x
Back-contact
Ray trace
Solar cell
High efficiency
Polyimide
IBC

ABSTRACT

Silicon solar cells incorporating double-sided pyramidal texture are capable of superior light trapping over cells with front-side only texture. However, increased surface area, roughness and exposed $\langle 111 \rangle$ crystal planes of textured surfaces not only causes increased recombination, but also makes cells susceptible to shunting through pinholes in the dielectric at the sharp peaks and valleys of the textured pyramids. A polyimide film as an insulating interlayer film is investigated to circumvent the tradeoff between improved light trapping, increased recombination and increased shunt paths. When applied at the rear of the interdigitated back contact silicon solar cell structure, the polyimide film provides an excellent electrical insulation ($> 1000 \text{ M}\Omega$ of insulation resistance) and increases photocurrent ($\sim 1.1 \text{ mA/cm}^2$) owing to an increased rear internal reflectance. The polyimide is also compatible with metal annealing of passivating dielectrics such as silicon nitride. Optical simulation and experimental results are combined in a 3D semiconductor simulation (Quokka) to quantify the possible gain of implementing the double-sided texture in high efficiency silicon solar cells.

1. Background

High-efficiency silicon solar cells typically have a textured front surface and a planar rear surface [1–5]. The light trapping in these structures suffers from the first-pass light rays incident to the rear surface being reflected into the escape cone of a front pyramid and coupled out [6]. Numerous light trapping schemes have been investigated to redirect rays such that a smaller fraction is reflected into the escape cone. These include the tiler's pattern [6]; perpendicular grooves [6]; a honeycomb texture realized by isotropic etching [1]; plasmonic nanoparticles on the rear of the wafer-based silicon solar cell structure [7]; a simple prism pyramidal texture realized by mechanical grooving [8]; a pigmented rear reflector [9]; dielectric back scattering [10]; diffused reflectors including white paint, titanium oxide nanoparticles, white backsheets and silver mirrors [11,12]; and a random pyramidal texture via alkaline etch solution [13] with and without chemical rounding [14]. Of these, the last scheme is the most widely-used and well-established method in the fabrication of silicon solar cells. The application of random pyramidal double-sided texture (DST) on the front and rear of silicon solar cells has been shown to provide superior light trapping relative to silicon solar cells with a textured front and a planar rear, as it helps to randomize the direction of light within the cell thereby reducing the chance of escape [6,14]. Note,

however, that the inclusion of rear pyramids is only preferable to planar when the rear internal reflectance R_{intR} is high; our simulations indicate that the threshold is $R_{intR} > 80\%$. As alkaline-assisted pyramidal texture is a relatively easy technique that is well-established in the PV industry, it offers a viable way to increase light trapping in crystalline silicon solar cells. Although rear texture also increases surface recombination and makes the rear surface more susceptible to shunting in cell structures such as interdigitated back contact (IBC) cells, using a chemical etch to round the rear pyramids mitigates those problems and higher cell efficiencies have been attained [15–21]; moreover, it has been concluded that when the etch duration is short, the chemical rounding has little influence on the overall light trapping [14]. In this paper, we present an investigation into the tradeoff between optical enhancement versus increased rear surface recombination and shunting for DST. The optical enhancement provided by different types of DSTs is examined via ray tracing. Recombination on pyramidal textured surfaces is investigated with plasma enhanced chemical vapor (PECVD) deposited silicon nitride (SiN_x). Incorporating polyimide (PI) as an electrically insulating film is introduced as a solution to the increased risk of recombination and shunts caused by DST in silicon solar cells. An investigation into its insulating quality, effects on carrier lifetime, and absorption in the polymer film is also presented. A comparison of cells with and without DST and PI is assessed by 3D Quokka simulation.

* Corresponding author at: University of Central Florida, Orlando, FL 32768, USA.
E-mail address: ngwe.zin@ucf.edu (N. Zin).

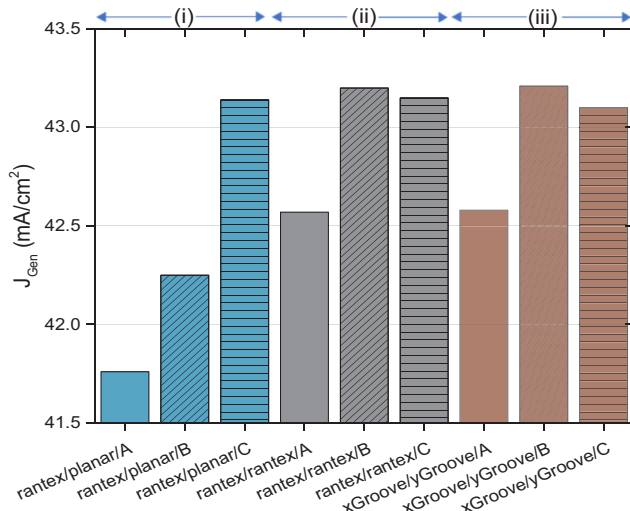


Fig. 1. J_{Gen} for a range of typical DST combinations. The parameters used are: normally incident AM1.5 G spectrum, a double-layer ARC (PECVD SiO_x and SiN_x of 80 nm and 75 nm, respectively) on the front surface, a 200 μm thick cell, and wavelength range of 300–1200 nm. Surface textures are referred to in the figure as ‘rantex’ for random pyramid texture, ‘x grooves’ for v-shaped grooves (52°) in ‘x’ direction, and ‘y grooves’ for v-shaped grooves (52°) in direction perpendicular to the ‘x’ direction. ‘A’ denotes that the internal reflection at the rear is specular and calculated for the case of films (a stack of 75 nm of SiN_x overlaid by 1000 nm of Al) coating the rear. ‘B’ denotes that the internal reflectance is 100% and specular. ‘C’ denotes that the internal reflectance is 100% reflection and Lambertian.

2. Optical enhancement of DST

Light trapping schemes in experimental high-efficiency silicon solar cells developed to date have had a textured front surface and a planar rear surface [2–5,22,23]. Numerous approaches have been presented to quantify the light trapping [6,24–31]. In the investigation carried out by Campbell and Green, the light trapping in silicon wafers was investigated for a number of structures such as (i) a textured front and a planar rear, (ii) pyramids on both sides, (iii) perpendicular grooves, (iv) a tiler’s pattern and (v) a shifted brickwork pattern [6]. As an extension to this study, we apply the PV Lighthouse ray tracer [32] to simulate the photogeneration current density J_{Gen} for structures (i), (ii) and (iii). The results are presented in Fig. 1 and details of the input parameters are included in the caption. The choice of the front and rear surface morphologies that we present is motivated by their fabrication feasibility. A Lambertian rear surface is included to represent an “ideal” rear surface scenario.

Consistent with [6], who evaluated the case of specular and 100% reflectance from the rear (Case B), we find that the perpendicular grooves yield the greatest advantage over a rantex/planar structure ($\Delta J_{Gen} \sim 1 \text{ mA/cm}^2$), but it is still only slightly superior to rantex/rantex, and this advantage is similar to that attained when the rear surface is Lambertian (Case C). We also find that when accounting for the rear films (Case A), ΔJ_{Gen} of these textures is reduced to $\sim 0.8 \text{ mA/cm}^2$. Simulations with alternative dielectric materials (e.g., SiO_2 , AlO_x , Si_3N_4) yielded similar trends. Thus, given the simplicity of its fabrication, rantex/rantex appears an excellent candidate for DST in commercial and laboratory silicon solar cells.

3. Application of DST with polyimide

Unfortunately, the benefit of improved light trapping by DST is offset by an increase in recombination due to its greater surface area, its sharp peaks and troughs, and (for some dielectrics) an exposure of $< 111 >$ facets [33–36]. Thus, the ultimate benefit to solar cells depends

strongly on the quality of the passivation. Two well-known and highly passivating films are PECVD SiN_x and ALD AlO_x , but these films do not provide robust insulation between metal and silicon substrate, and they are not suitable to be used as an insulating layer between the metal and textured or diffused silicon due to high leakage currents and low dielectric breakdown voltage [37]. This can lead to a poor shunt resistance and an increase in recombination. Shunting is also one of the major obstacles resulting in poor conversion efficiency in research and manufacturing of high efficiency IBC silicon solar cells [38]. We therefore explore the use of polyimide (PI) as an insulation layer between the metal and the dielectric films, testing its insulation properties and its effect on surface passivation and optics.

3.1. Polyimide

Polyimide (PI) films have been used as stress buffer layers, interlayer dielectrics, and protecting films in microelectronic applications [39–41]. PI films also have excellent mechanical properties allowing them to survive the thermal and chemical exposures of post-application processing, good elongation property that prevents cracking, and excellent adhesion to a wide range of metals. In addition, PIs are patternable by photolithography [42,43] and have been demonstrated as an interlayer dielectric for double-level metallization [44]. The PI films discussed herein appear to be well-suited as interlayer insulators between textured pyramids coated by low temperature passivation dielectrics and the rear metal.

3.2. Electrical insulation

The insulation capability of PI (HD-4100) was investigated by fabricating a heavy phosphorus diffusion ($40 \Omega/\square$) on symmetrically textured low-resistivity ($1.5 \Omega\text{-cm}$) $\sim 250 \mu\text{m}$ thick n-type silicon, and spin-coating 2–3 μm of PI onto the front side at 5000 rpm for 30 s and curing it at 350°C in nitrogen for 30 min. Aluminum (Al) pads ($\sim 1 \mu\text{m}$ thick and 1 cm^2) were then evaporated on both sides of the sample, followed by sintering the samples in a forming gas environment at 250°C for 30 min to ensure the Al was alloyed with the phosphorus-doped silicon at the rear. The presence of the heavy phosphorus diffusion ensured the contact resistivity between the Al and silicon substrate at the rear was negligible. The current-voltage characteristics were then measured using the 4-point probe method, contacting positive polarity probes to the Al pad on top and negative probes to the pad on the rear or vice versa to determine the total resistance. The average resistance measured across six test structures was $\sim 7.7 \times 10^9 \Omega$ with a standard deviation of $3 \times 10^9 \Omega$. In comparison, an insulation provided by a stack of SiO_2 and LPCVD Si_3N_4 films on interdigitated back contact cell structures [3,45–51] has an average resistance of $\sim 1 \times 10^7 \Omega$. The very high resistance of the PI film suggests that it is well-suited as an insulation layer between metal and textured pyramids.

3.3. Surface recombination

We employed undiffused high-resistivity n-type FZ $< 100 > 100 \Omega\text{-cm}$ silicon wafers that were textured with random upright pyramids and passivated with PECVD SiN_x ($\sim 75 \text{ nm}$). The J_0 measurements were determined by a photoconductance decay (PCD) instrument following the Kane and Swanson technique [52], assuming an intrinsic carrier concentration of $n_i = 8.95 \times 10^9 \text{ cm}^{-3}$ (at 297 K). The measured J_0 was 7 fA/cm^2 (per side), which is typical of high-performing dielectric passivation on texture [33,34,36].

The PI film was then applied on both sides of the SiN_x coated samples at 5000 rpm for 30 s, followed by annealing in a nitrogen ambient at 300°C , 325°C , and 350°C for 30 min and 60 min. The purpose of the nitrogen anneal is to mimic the imidization of PI film following the cure. Imidization refers to the conversion of a polyimide into an imide by heat (or a catalyst) through the reaction process that

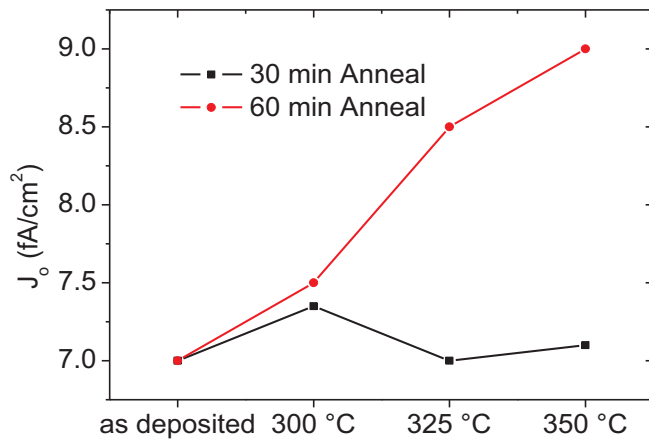


Fig. 2. J_0 measurement of SiN_x passivated samples following PI coat and cure at different temperatures and times. PI has a post-cure thickness of ~ 2000 – 3000 nm.

reduces the polymer solubility and produces water as a by-product, which in turn reacts with remaining polymeric acid, thereby cleaving the polymer chain.

Fig. 2 shows that the J_0 remained stable for PI coated SiN_x samples when subjected to 30 min of imidization for a range of temperature between 300 and 350 °C, however, 60 min of imidization shows some increase in J_0 . The cause of this could be due to dehydrogenation triggered by the long annealing time. This experiment demonstrates that the application of a PI film with an imidization time to 30 min has no adverse effects on the passivation quality of PECVD SiN_x film, and that a low J_0 can be maintained.

3.4. Light trapping

Since the application of PI is at the rear of a silicon solar cell, the benefits of light trapping by the rear texture can be altered by the PI. To assess the effect of the PI on light trapping, samples that mimic the cell structure with and without PI at the rear were prepared. Fig. 3(a) presents a schematic of the samples, while Fig. 3(b) and (c) present scanning electron microscopic images of random pyramidal textured silicon coated with or without PI. Fig. 3(c) shows that the PI is partially conformal to the textured pyramidal surface.

The hemispherical reflectance of both samples is plotted as symbols in Fig. 4(a). The figure shows that adding PI to the rear leads to more light escaping from the solar cell. To assess the reason for this difference, and to estimate the difference in absorption within the silicon, these samples were simulated using the PV Lighthouse SunSolve ray-tracing program. The characteristic angle of the pyramids was set to 53°, which is typical of the random pyramids fabricated in our laboratory [53]. The complex refractive index (n and k) of PI was taken from the manufacturer (shown in Fig. 1 of the Supplementary material), and the complex refractive index of Si [54], SiN_x [55] (with $n = 1.96$ at 632 nm), and Al [56] was taken from the literature. Additional details of the simulation inputs are provided in Table 1–5 of the Supplementary material. Note that, as displayed in Fig. 3(a), it is assumed that the PI is conformal to the rear pyramids in this initial simulation.

As evident in Fig. 4(a), the measured and ray-traced escape reflectance agree well. This provides some confidence that the ray-tracing model represents the experimental samples, and that the simulated absorptance within the silicon (which cannot be measured directly) is also representative of the samples. This absorptance is plotted in Fig. 4(b) for samples with a textured and planar rear, as well as for the case of a non-conformal PI (see Table 5 of the Supplementary material for inputs).

The following can be construed from Fig. 4(b):

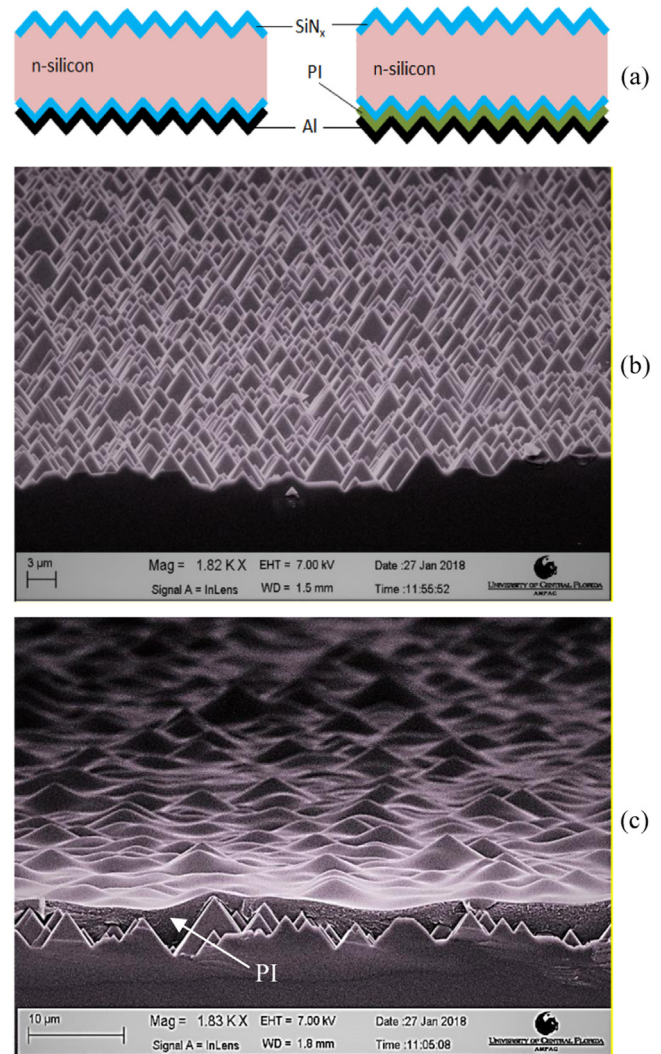


Fig. 3. (a) The solar cell structures incorporating PI at the rear of the textured pyramids used for ray tracing, SEM images of (b) random pyramidal textured and (c) PI-coated random pyramidal textured samples, measured by Zeiss ULTRA-55.

- (i) Consistent with previous studies (e.g., [6,14]), introducing texture at the rear surface leads to a significant increase in the absorption within the silicon (for samples with a high rear-internal reflectance). This improvement is evident for samples with or without the PI.
- (ii) When PI is included at a textured rear it leads to a notable increase in absorption within the silicon. The reason for this improvement is that the rear internal reflectance increases due to the PI being thick, having a relatively low refractive index, and being lowly absorbing, which reduces absorption in the Al [57]. A recently published paper also notes that a polymer on the rear of IBC cell can increase the optical gain [58]. The simulated generation current J_{Gen} when the PI is included, increases by 0.3 mA/cm^2 under the AM1.5g spectrum.
- (iii) When the PI is included at a planar rear, it leads to a minor increase in absorption in the silicon of $\Delta J_{Gen} = 0.4 \text{ mA/cm}^2$. The improvement is due to a higher reflectance at the rear, but the PI makes less of an impact than when deposited on texture because for a planar surface, most of the first-pass rays are total-internally reflected at the rear irrespective of whether the rear has the PI. Hence the increase in absorption is more evident at longer wavelengths because long-wavelength rays are more likely to interact

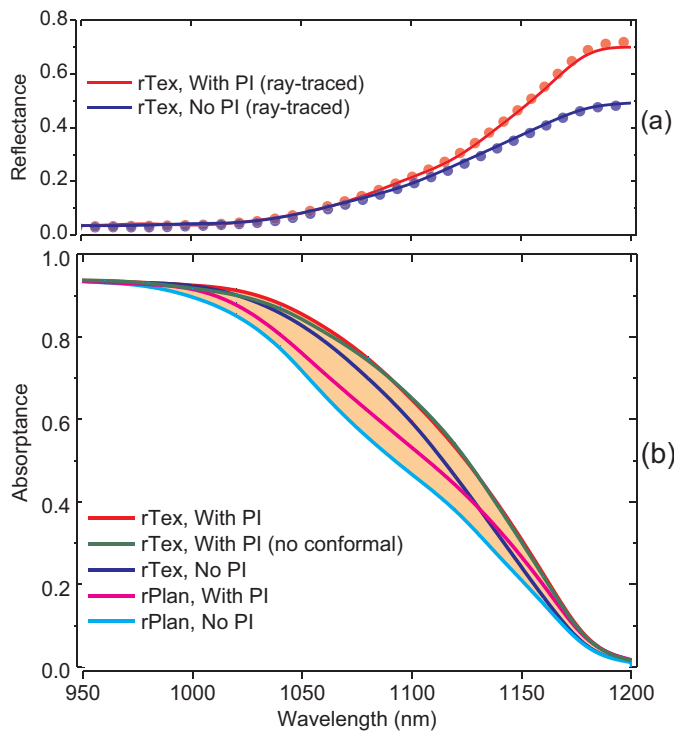


Fig. 4. (a) the hemispherical reflectance (measured and simulated), and (b) the simulated absorbance of structures having a stack of SiN_x, Si (rTex or rPlan), SiN_x and Al, with or without PI at the rear. Dotted and solid lines show measured and simulated data, respectively. In the legend, ‘rTex’, ‘rPlan’, denote rear random pyramidal texture, rear planar. Silicon and SiN_x have the thickness of 195 μm and 75 nm, respectively. All structures measured and ray-traced have pyramidal texture on the front side.

multiple times with the rear surface.

- (iv) Introducing both texture and PI to the rear (i.e. compared to a planar rear without PI) leads to a large improvement in absorbance, equivalent to $\Delta J_{Gen} = 1.1 \text{ mA/cm}^2$.
- (v) When the rear surface of the PI is flat (green line) rather than conformal (red line) it makes little change to the absorbance. The PI is thick enough in both cases (compare Table 1 and 5 of the Supplementary material) that the evanescent absorption in the Al is minimal. The difference between the scenarios equates to just $\Delta J_{Gen} = 0.01 \text{ mA/cm}^2$. If the PI were even thinner than 1 μm at the peaks of the pyramids, and hence there was more absorption at those peaks, those regions still only contribute to a small fraction of the total surface area. The similarity between these curves, which represent the ideal cases of the PI being purely conformal and having a planar rear, suggest that the absorbance of the actual sample (see Fig. 3(c)) would also be similar. The agreement between simulation and experiment in Fig. 4(b) supports this conclusion (Fig. 5).

4. Electro-optical simulation

To further quantify the benefits of incorporating DST into solar cells, the performance of n-type interdigitated back contact (IBC) cell structures, having an identical textured front surface but the rear planar coated with or without PI and the rear pyramidal texture coated with PI, was determined by Quokka [59]. The IBC structure has SiN_x as a passivation layer on both the front and rear surfaces. Input parameters and 3-dimensional device structures used for the simulation of the IBC are shown in Table 6 of the Supplementary material. J_{Gen} is separately obtained by the module ray tracer in conjunction with OPAL 2 [32], and used as an input to the simulation. Table 1 shows the simulated

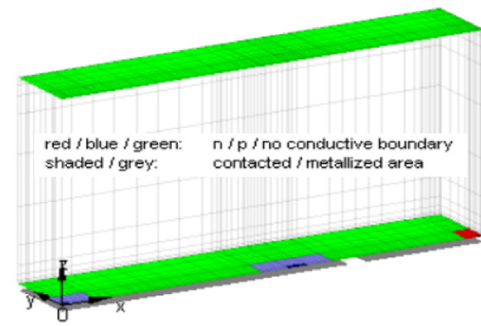


Fig. 5. Device structures of IBC cell for 3-dimensional device Quokka simulation.

Table 1

Electrical parameters of IBC solar cells simulated with and without rear texture.

		V _{oc} (V)	J _{sc} (mA/cm ²)	FF (%)	η (%)
1.	Textured rear with PI	711	42.9	81.4	24.9
2.	Planar rear with PI	717	42.3	81.7	24.8
3.	Planar rear without PI	717	41.9	81.7	24.6

conversion efficiency of the IBC cell incorporating pyramidal texture and planar rear surfaces. The simulation suggests that the increase in surface current generation and recombination combined reduces V_{oc} by 6 mV and FF by 0.3% (rel), but this reduction does not completely offset the gain in J_{sc}. The study suggests that the incorporation of rear pyramids and a polyimide insulation layer into high-efficiency IBC solar cells would yield a net benefit to efficiency of + 0.3%. In addition, incorporating PI at the rear of the cell with just the front side textured would yield a conversion efficiency of 0.2% higher than that without PI at the rear, thanks to its moderate increase in J_{sc} and an uncompromised V_{oc}, as its surface being planar.

5. Conclusion

The application of DST and a rear PI insulation film to increase the silicon solar cell efficiency was investigated. The PI between metal and passivated textured surface of DST structures demonstrated (i) an excellent insulation resistance (> 1000 MΩ) between metal and dielectric layer (ii) little degradation in passivation quality, and (iii) an increased absorption within the silicon ($\Delta J_{Gen} = 1.1 \text{ mA/cm}^2$ compared to the structure with a planar rear and no PI). Three-dimensional simulation suggests that including PI at the rear would increase the conversion efficiency of laboratory-style IBC cells with a planar and textured rear surface by 0.2% and 0.3%, respectively.

Acknowledgement

Prof. Pieter G. Kik of the College of Optics & Photonics, University of Central Florida for the fruitful discussion and suggestion of PI film measurement. Carl Wittbecker of the Dupont HD Microsystems for the optical data of HD-4100 film. The funding of this research is supported by the Florida Renewable Energy Efficiency Technologies grant of SO430/24608, and the Australian Solar Institute (now known as Australian Government through the Australian Renewable Energy Agency, ARENA) through research grants of 4-F002 and RND009. This research is partially funded by Trina Solar. Responsibility for the views, information or advice expressed herein is not accepted by the Office of Energy, Florida and Australian Government.

Appendix A. Supplementary material

Supplementary data associated with this article can be found in the

online version at <http://dx.doi.org/10.1016/j.solmat.2018.03.015>.

References

- [1] J. Zhao, A. Wang, P. Campbell, M.A. Green, A 19.8% efficient honeycomb multi-crystalline silicon solar cell with improved light trapping, *IEEE Trans. Electron Devices* 46 (10) (1999) 1978–1983.
- [2] J. Zhao, Passivated emitter rear locally diffused solar cells, *Bull. Adv. Technol. Res.* (2011) 41–43.
- [3] E. Franklin, et al., Design, fabrication and characterisation of a 24.4% efficient interdigitated back contact solar cell, *Prog. Photovolt.: Res. Appl.* (2014).
- [4] K. Masuko, et al., Achievement of more than 25% conversion efficiency with crystalline silicon heterojunction solar cell, in: 40th IEEE PVSC, Colorado, Denver, 2014.
- [5] J. Nakamura, et al., Development of Heterojunction Back Contact Si Solar Cells, in: Proceedings of the 40th IEEE Photovoltaics Specialist Conference, Denver, Colorado, 2014.
- [6] P. Campbell, M. Green, Light trapping properties of pyramidally textured surfaces, *J. Appl. Phys.* (1987).
- [7] C. Barugkin, Z. Ngwe-Soe, K.R. Catchpole, Photoluminescence enhancement towards high efficiency plasmonic solar cells, Presented at the Photovoltaic Specialists Conference (PVSC), 2013 IEEE 39th, 16–21 June 2013.
- [8] R. Brendel, Simple prism pyramids: a new light trapping texture for silicon solar cells, Presented at the Photovoltaic Specialists Conference, 1993, Conference Record of the Twenty Third IEEE, 10–14 May 1993.
- [9] J.E. Cotter, Optical intensity of light in layers of silicon with rear diffuse reflectors, *J. Appl. Phys.* 84 (1) (1998) 618–624.
- [10] M. v. Lare, F. Lenzmann, A. Polman, Dielectric back scattering patterns for light trapping in thin-film Si solar cells, *Opt. Express* (2013).
- [11] J. Frank, M. Rüdiger, S. Fischer, J.C. Goldschmidt, M. Hermle, Optical simulation of bifacial solar cells, *Energy Procedia* 27 (Suppl. C) (2012) 300–305 (2012/01/01/).
- [12] F. Pfeiffer, J. Eisenlohr, A. Basch, M. Hermle, B.G. Lee, J.C. Goldschmidt, Systematic analysis of diffuse rear reflectors for enhanced light trapping in silicon solar cells, *Sol. Energy Mater. Sol. Cells* 152 (Suppl. C) (2016) 80–86 (2016/08/01/).
- [13] J. Haynos, J. Allison, R. Arndt, L. Meulenberg, The COMSAT non-reflective silicon solar cell: a second generation improved cell, Presented at the International Conference on Photovoltaic Power Generation, Hamberg, 1974.
- [14] K.R. McIntosh, et al., Optical evaluation of silicon wafers with rounded rear pyramids, *IEEE J. Photovolt.* 7 (6) (2017) 1596–1602.
- [15] A. Cacciato, et al., Investigating manufacturing options for industrial PERL-type Si solar cells, *Sol. Energy Mater. Sol. Cells* 113 (2013) 153–159 (2013/06/01/).
- [16] J. Horzel et al., Development of rear side polishing adapted to advanced solar cell concepts, in: Proceedings of the 26th European Photovoltaic Solar Energy Conference and Exhibition, 2011, pp. 2210–2216.
- [17] T. Schwab, et al., Recombination and optical properties of wet chemically polished thermal oxide passivated Si surfaces, *IEEE J. Photovolt.* 3 (2) (2013) 613–620.
- [18] C. Kranz, et al., Wet chemical polishing for industrial type PERC solar cells, *Energy Procedia* 38 (2013) 243–249 (2013/01/01/).
- [19] C. Kranz et al., Impact of the rear surface roughness on industrial-type PERC solar cells, in: Proceedings of the 27th European Photovoltaic Solar Energy Conference and Exhibition, 2012, pp. 557–560.
- [20] E. Cornagliotti et al., How much rear side polishing is required? A study on the impact of rear side polishing in PERC solar cells, in: Proceedings of the 27th European Photovoltaic Solar Energy Conference and Exhibition, 2012, pp. 561–566.
- [21] A. Dastgheib-Shirazi, M. Steyer, J. Junge, S. Gindner, G. Hahn, A study of the surface morphology of silicon: effect of parasitic emitter etching on the rear side performance of silicon solar cells, in: Proceedings of the 25th European Photovoltaic Solar Energy Conference and Exhibition and 5th World Conference on Photovoltaic Energy Conversion, 2010, pp. 2107–2113.
- [22] J. Zhao, A. Wang, M.A. Green, 24.5% Efficiency silicon PERT cells on MCZ substrates and 24.7% efficiency PERL cells on FZ substrates, *Prog. Photovolt.: Res. Appl.* 7 (6) (1999) 471–474.
- [23] C. Reichel, F. Granek, M. Hermle, S.W. Glunz, Back-contacted back-junction n-type silicon solar cells featuring an insulating thin film for decoupling charge carrier collection and metallization geometry, *Prog. Photovolt.: Res. Appl.* 21 (5) (2013) 1063–1076.
- [24] J.A. Rand, P.A. Basore, Light-trapping silicon solar cells-experimental results and analysis, in: Photovoltaic Specialists Conference, 1991, Conference Record of the Twenty Second IEEE, 1991, pp. 192–197 vol.1.
- [25] P.A. Basore, Extended spectral analysis of internal quantum efficiency, in: Proceedings of the 23rd IEEE Photovoltaic Specialist Conference, Louisville, KY, USA, 1993, pp. 147–152.
- [26] Z. Liu, N. Sahaie, B. Hoex, A.G. Aberle, I.M. Peters, Optical modeling of alkaline saw-damage-etched rear surfaces of monocrystalline silicon solar cells, *IEEE J. Photovolt.* 4 (6) (2014) 1436–1444.
- [27] R. Brendel, M. Hirsch, R. Plieninger, J.H. Werner, Quantum efficiency analysis of thin-layer silicon solar cells with back surface fields and optical confinement, *IEEE Trans. Electron Devices* 43 (7) (1996) 1104–1113.
- [28] S. Pillai, K.R. Catchpole, T. Trupke, M.A. Green, Surface plasmon enhanced silicon solar cells, *J. Appl. Phys.* 101 (9) (2007) 093105.
- [29] V.E. Ferry, et al., Light trapping in ultrathin plasmonic solar cells, *Optics Express* 18 (S2) (2010) A237–A245 (2010/06/21).
- [30] K.R. McIntosh, N. Shaw, J.E. Cotter, Light trapping in SunPower's rear-contact solar cells, in: Proceedings of the 19th Europe Photovoltaic Solar Energy Conference and Exhibition, Paris, France, 2004, pp. 844–847.
- [31] K.R. McIntosh, S.C. Baker-Finch, A parameterization of light trapping in wafer-based solar cells, *IEEE J. Photovolt.* 5 (6) (2015) 1563–1570.
- [32] P. Lighthouse. Available <www.pvlighthouse.com.au>.
- [33] Y. Wan, K.R. McIntosh, On the surface passivation of textured C-Si by PECVD silicon nitride, *IEEE J. Photovolt.* 3 (4) (2013) 1229–1235.
- [34] S.C. Baker-Finch, K.R. McIntosh, The contribution of planes, vertices, and edges to recombination at pyramidally textured surfaces, *IEEE J. Photovolt.* 1 (1) (2011) 59–65.
- [35] K.R. McIntosh, L.P. Johnson, Recombination at textured silicon surfaces passivated with silicon dioxide, *J. Appl. Phys.* 105 (12) (2009) 124520.
- [36] L.E. Black, New Perspectives on Surface Passivation: Understanding the Si–Al₂O₃ Interface (Ph.D. dissertation), Australian National University, 2015 (Chapter 8).
- [37] J. Yota, Effects of deposition method of PECVD silicon nitride as mim capacitor dielectric for GaAs HBT technology, in: Symposium on Silicon Nitride, Silicon Dioxide, and Emerging Dielectrics of the 2011 Electrochemical Society (ECS) Meeting, Montreal, Canada, 2011.
- [38] C.E. Chan, B.J. Hallam, S.R. Wenham, Simplified interdigitated back contact solar cells, *Energy Procedia* 27 (0) (// 2012) 543–548.
- [39] F. Bossuyt, T. Vervust, F. Axisa, J. Vanfleteren, Improved stretchable electronics technology for large area applications, *MRS Proc.* 1271 (2010) (Art. no. 1271-1j08-03).
- [40] M.E. Grady, P.H. Geubelle, N.R. Sottos, Interfacial adhesion of photodefinable polyimide films on passivated silicon, *Thin Solid Films* 552 (Suppl. C) (2014) 116–123 (2014/02/03/).
- [41] K. Zoschke, et al., Wafer level processing of integrated passive components using polyimide or polybenzoxazole/copper multilayer technology, *IEEE Trans. Adv. Packag.* 33 (2) (2010) 398–407.
- [42] B.T. David, et al., Flexible superconducting Nb transmission lines on thin film polyimide for quantum computing applications, *Supercond. Sci. Technol.* 29 (8) (2016) 084007.
- [43] W.-C. Choi, Polymer micromachined flexible tactile sensor for three-axial loads detection, *Trans. Electr. Electron. Mater.* 11 (2010) 130–133.
- [44] P.J. Verlinden, R.M. Swanson, R.A. Crane, 7000 high-efficiency cells for a dream, *Prog. Photovolt.: Res. Appl.* 2 (2) (1994) 143–152.
- [45] N. Zin, Andrew Blakers, Keith McIntosh, Evan Franklin, Teng Kho, Johnson Wong, Thomas Mueller, Armin G. Aberle, Zhiqiang Feng, Qiang Huang, 19% efficient n-type all-back-contact silicon wafer solar cells with planar front surface, in: Australian Solar Energy Society Conference, Sydney, Australia, 2011.
- [46] N. Zin, A. Blakers, E. Franklin, T. Kho, K. Chern, K. McIntosh, J. Wong, T. Mueller, A.G. Aberle, Y. Yang, X. Zhang, Z. Feng, Q. Huang, Laser-assisted shunt removal on high-efficiency silicon solar cells, in: Proceedings of the 27th European Photovoltaic Solar Energy Conference and Exhibition, Frankfurt, Germany, 2012.
- [47] N. Zin, et al., Progress in the development of all-back-contacted silicon solar cells, *Energy Procedia* 25 (2012) 1–9.
- [48] N. Zin, et al., Continued development of all-back-contact silicon wafer solar cells at ANU, *Energy Procedia* 33 (2013) 50–63.
- [49] N. Zin, et al., Rounded rear pyramidal texture for high efficiency silicon solar cells, in: Proceedings of the 43rd IEEE Photovoltaics Specialist Conference Portland, Oregon, 2016.
- [50] A. Blakers, et al., 24.6% efficient back contact cell with oxide-nitride passivation, in: Proceedings of the 23rd International Photovoltaic Science and Engineering Conference, Taipei, Taiwan, 2013.
- [51] N. Zin, Recombination-free reactive ion etch for high efficiency silicon solar cells, *Sol. Energy Mater. Sol. Cells* 172 (2017) 55–58.
- [52] D.E. Kane, R.M. Swanson, Measurement of the emitter saturation current by a contactless photoconductivity decay method, in: Proceedings of the 18th IEEE Photovoltaic Specialist Conference, Las Vegas, 1985, pp. 578–583.
- [53] K.R. McIntosh et al., Quantifying the optical losses in back-contact solar cells, in: IEEE Proceedings of the 40th Photovoltaic Specialist Conference (PVSC), 2014, pp. 0115–0123.
- [54] M.A. Green, Self-consistent optical parameters of intrinsic silicon at 300K including temperature coefficients, *Sol. Energy Mater. Sol. Cells* 92 (11) (2008) 1305–1310 (2008/11/01/).
- [55] S. Duttagupta, F. Ma, B. Hoex, T. Mueller, A.G. Aberle, Optimised antireflection coatings using silicon nitride on textured silicon surfaces based on measurements and multidimensional modelling, *Energy Procedia* 15 (2012) 78–83 (2012/01/01/).
- [56] E. Palik, Handbook of Optical Constants of Solids, Academic Press, Orlando, 1985, pp. 397–400.
- [57] K.O. Davis, et al., Investigation of the internal back reflectance of rear-side dielectric stacks for c-Si solar cells, *IEEE J. Photovolt.* 3 (2) (2013) 641–648.
- [58] Z. Li, Y. Li, Z. Ouyang, P.-C. Hsiao, Y. Jiang, A. Lennon, Electrical and optical analysis of polymer rear insulation layers for back contact cells, Presented at the 5th International Conference on Silicon Photovoltaics, SiliconPV 2015, Konstanz, Germany, 2015.
- [59] A. Fell, A free and fast 3D/2D solar cell simulator featuring conductive boundary and quasi-neutrality approximations, *IEEE Trans. Electron Devices* 60 (2) (2012) 733–738.

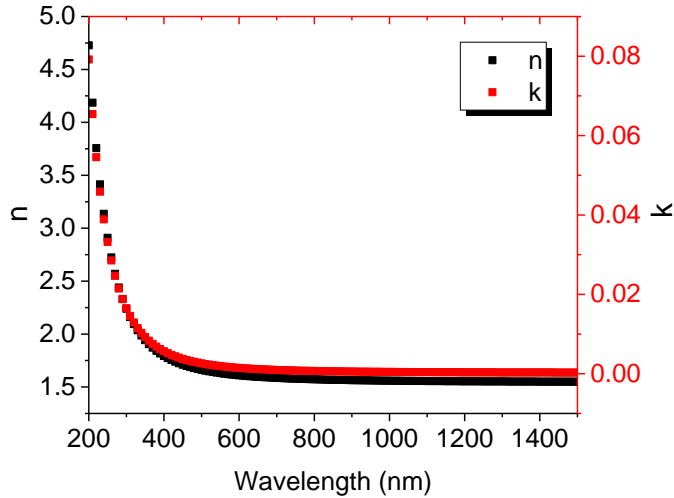


FIG 1: Measured refractive index n and extinction coefficient k of HD-4100 polyimide film.

Table 1: Parameters used in ray tracing the reflectance and absorptance for double-sided texture cell structure of $\text{SiN}_x/\text{Si}/\text{SiN}_x/\text{PI}/\text{Al}$ in FIG 4.

Spectrum	AM1.5G		Wavelength (300 - 1200 nm)	
	Morphology	Angle ($^\circ$)	Height/Width (μm)	Lambertian
Front	random upright	53	3.3/4.973	
Rear	random upright	53	3.3/4.973	0.9
	Material	Thickness (nm)		
Front Film #1	SiN_x	75		
Substrate	Si	195		
Rear Film #1	SiN_x	75		
Rear Film #2	PI	2000		
Rear Film #3	Al	1000		

Table 2: Parameters used in ray tracing the reflectance and absorptance for double-sided texture cell structure of $\text{SiN}_x/\text{Si}/\text{SiN}_x/\text{Al}$ in FIG 4.

Spectrum	AM1.5G		Wavelength (300 - 1200 nm)	
	Morphology	Angle ($^\circ$)	Height/Width (μm)	Lambertian
Front	random upright	53	3.3/4.973	
Rear	random upright	53	3.3/4.973	0.9
	Material	Thickness (nm)		
Front Film #1	SiN_x	75		
Substrate	Si	195		
Rear Film #1	SiN_x	75		
Rear Film #2	Al	1000		

Table 3: Parameters used in ray tracing the reflectance and absorptance for front-side textured and rear planar cell structure of SiN_x/Si/SiN_x/Al in FIG 4.

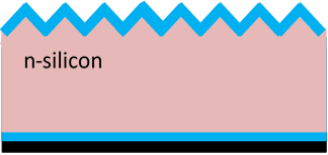
Spectrum	AM1.5G	Wavelength (300 - 1200 nm)		
	Morphology	Angle (°)	Height/Width (μm)	Lambertian
Front	random upright	53	3.3/4.973	
Rear	planar			0
	Material	Thickness (nm)		
Front Film #1	SiN _x	75		
Substrate	Si	195		
Rear Film #1	SiN _x	75		
Rear Film #2	Al	1000		

Table 4: Parameters used in ray tracing the reflectance and absorptance for front-side textured and rear planar cell structure of SiN_x/Si/SiN_x/PI/Al in FIG 4.

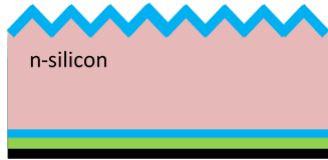
Spectrum	AM1.5G	Wavelength (300 - 1200 nm)		
	Morphology	Angle (°)	Height/Width (μm)	Lambertian
Front	random upright	53	3.3/4.973	
Rear	planar			0
	Material	Thickness (nm)		
Front Film #1	SiN _x	75		
Substrate	Si	195		
Rear Film #1	SiN _x	75		
Rear Film #2	PI	2000		
Rear Film #3	Al	1000		

Table 5: Parameters used in ray tracing the reflectance and absorptance for double-sided texture cell structure of SiN_x/Si/SiN_x/non-conformal PI/Al in FIG 4.

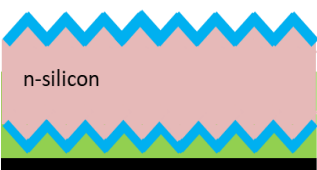
Spectrum	AM1.5G	Wavelength (300 - 1200 nm)		
	Morphology	Angle (°)	Height/Width (μm)	Lambertian
Front	random upright	53	3.3/4.973	
Rear	random upright	53	3.3/4.973	0.9
	Material	Thickness (nm)		
Front Film #1	SiN _x	75		
Substrate	Si	195		
Rear Film #1	SiN _x	75		
Rear Layer #1	PI	3000		
Rear Layer #2	Al	1000		

Table 6: Input parameters for 3D Quokka simulation of IBC Device shown in FIG 4.

	Parameters
Cell size	2 x 2 cm ²
Cell thickness	240 μm
Bulk type	n-type
Bulk resistivity	100 Ω.cm
Bulk SRH lifetime	8000 μs
Front films	75 nm PECVD SiN _x
Front morphology	see table 2 for DST structure see table 4 and 5 for front-side only textured
Front diffusion	Undiffused, passivated
Front recombination (J_o)	Passivated, 7 fA/cm ²
Rear films	see table 2 for DST structure see table 4 and 5 for front-side only textured
Rear pitch	500 μm
P-diffusion diameter	30 μm
P-diffusion pitch	140 μm
n-diffusion diameter	30 μm
n-diffusion pitch	70 μm
Rear contacts opening	7 μm wide
Rear n-diffusion R_{sh}	20 Ω/□
n-diffusion J_o	Passivated, 300 fA/cm ² Contacted, 180 fA/cm ²
n-contact resistivity	1.2 x 10 ⁻⁵ Ω·cm ²
Rear p-diffusion R_{sh}	80 Ω/□
p-diffusion J_o	Passivated, 95 fA/cm ² Contacted, 1000 fA/cm ²
-contact resistivity	2 x 10 ⁻⁵ Ω·cm ²
Rear surface J_o	Undiffused, passivated, 7 fA/cm ² for textured 3 fA/cm ² for planar
Rear morphology	see table 2 for DST structure see table 4 and 5 for front-side only textured
Rear films	see table 2 for DST structure see table 4 and 5 for front-side only textured